PUBLICATION III

Crystal structure of an ascomycete fungal laccase from *Thielavia arenaria* – common structural features of asco-laccases

In: FEBS Journal 278(2011), pp. 2283–2295.

the FEBS Journal

Crystal structure of an ascomycete fungal laccase from *Thielavia arenaria* – common structural features of asco-laccases

Juha P. Kallio[1], Chiara Gasparetti[2], Martina Andberg[2], Harry Boer[2], Anu Koivula[2], Kristiina Kruus[2], Juha Rouvinen[1] and Nina Hakulinen[1]

1 Department of Chemistry, University of Eastern Finland, Joensuu, Finland
2 VTT Technical Research Centre of Finland, Espoo, Finland

Keywords
ascomycete; C-terminal plug; laccase; proton transfer; redox potential

Correspondence
N. Hakulinen, Department of Chemistry, University of Eastern Finland, Joensuu Campus, P.O. Box 111, FIN-80101 Joensuu, Finland
Fax: +358 13 2513390
Tel: +358 13 2513359
E-mail: nina.hakulinen@uef.fi

(Received 8 March 2011, revised 20 April 2011, accepted 27 April 2011)

doi:10.1111/j.1742-4658.2011.08146.x

Laccases are copper-containing enzymes used in various applications, such as textile bleaching. Several crystal structures of laccases from fungi and bacteria are available, but ascomycete types of fungal laccases (asco-laccases) have been rather unexplored, and to date only the crystal structure of *Melanocarpus albomyces* laccase (MaL) has been published. We have now solved the crystal structure of another asco-laccase, from *Thielavia arenaria* (TaLcc1), at 2.5 Å resolution. The loops near the T1 copper, forming the substrate-binding pockets of the two asco-laccases, differ to some extent, and include the amino acid thought to be responsible for catalytic proton transfer, which is Asp in TaLcc1, and Glu in MaL. In addition, the crystal structure of TaLcc1 does not have a chloride attached to the T2 copper, as observed in the crystal structure of MaL. The unique feature of TaLcc1 and MaL as compared with other laccases structures is that, in both structures, the processed C-terminus blocks the T3 solvent channel leading towards the trinuclear centre, suggesting a common functional role for this conserved 'C-terminal plug'. We propose that the asco-laccases utilize the C-terminal carboxylic group in proton transfer processes, as has been suggested for Glu498 in the CotA laccase from *Bacillus subtilis*. The crystal structure of TaLcc1 also shows the formation of a similar weak homodimer, as observed for MaL, that may determine the properties of these asco-laccases at high protein concentrations.

Database
Structural data are available in the Protein Data Bank database under the accession numbers 3PPS and 2VDZ

Structured digital abstract
- **laccase** binds to **laccase** by x-ray crystallography (View interaction)

Introduction

Laccases (benzenediol oxygen oxidoreductases) are enzymes belonging to the group of blue multicopper oxidases, along with ascorbate oxidases [1], mammalian plasma ceruloplasmin [2], *Escherichia coli* copper

Abbreviations
ABTS, 2,2′-azinobis(3-ethylbenzo-6-thiazolinesulfonic acid); BsL, *Bacillus subtilis* laccase; 2,6-DMP, 2,6-dimethoxyphenol; MaL, *Melanocarpus albomyces* laccase; PDB, Protein Data Bank; RlL, *Rigidoporus lignosus* laccase; rMaL, recombinant *Melanocarpus albomyces* laccase; TaLcc1, *Thielavia arenaria* laccase; ThL, *Trametes hirsuta* laccase; TvL, *Trametes versicolor* laccase.

efflux operon, which is involved in copper homeostasis [3], a yeast plasma membrane-bound Fet3p that catalyses iron oxidation [4], and phenoxazinone synthase from *Streptomyces antibioticus* [5]. Laccases are common in fungi, and are also found in some higher plants and bacteria. These enzymes are capable of oxidizing various organic and even inorganic substrates; however, in general, their substrates are phenolic compounds (such as those presented in Table 1). Phenolics are oxidized near the T1 copper to phenoxy radicals, which can then form a large variety of oxidation products by radical reactions. The substrate variety can be increased by the use of redox mediators, such as 2,2′-azinobis(3-ethylbenzo-6-thiazolinesulfonic acid) (ABTS). In addition, direct electron exchange between laccase and, for example, graphite electrodes [6,7] has been reported. The broad substrate range, wide pH optimum and thermostability of some laccases, as well as their use of oxygen as the terminal electron acceptor, mean that these enzymes have great potential for several applications, such as pulp bleaching, textile dye decolorization, delignification, bioremediation, fuel cells, and sensors [8,9].

Laccases have recently been extensively studied by X-ray crystallography. The first complete laccase structures were published in 2002, and crystal structures from at least 10 different organisms have now been reported. Most of the structures are from sporophoral basidiomycota fungi: *Coprinus cinereus* [10], *Trametes versicolor* [11,12], *Rigidoporus lignosus* [13], *Cerrena maxima* [14], *Coriolus zonatus* [15], *Lentinus tigrinus* [16], *Trametes trogii* [17], *Trametes hirsuta* [18], and *Coriolopsis gallica*. Structures of bacterial laccases or multicopper oxidases are also available, including the spore coat protein A from *Bacillus subtilis* [20], a copper efflux operob from *E. coli* [21], and the more recently published novel two-domain laccases [22–24]. The other phylum of the fungi, the Ascomycota or sac fungi, is much less studied, and only the crystal structure of *Melanocarpus albomyces* laccase (MaL) has been solved [25].

The fold of the three-domain laccases is composed of three β-barrel domains that are assembled around two catalytic copper-binding sites (Fig. 1). The active sites are formed by four copper cations, which are divided into three different types – type 1 (T1), type 2 (T2), and type 3 (T3) – by their characteristic spectro-

Table 1. Kinetic parameters for rMaL, TaLcc1, and ThL, measured with 2,6-DMP, syringic acid and methyl syringate in 25 mM succinate buffer at pH 4.5 and in 40 mM Mes buffer at pH 6.0 (25 °C). Structural formulas of the substrates are presented. Redox potentials (E°) of T1 coppers of the laccases and redox potentials of the substrates at pH 4.5 and pH 6.0 are provided, together with the redox potential differences (ΔE°) between the T1 coppers of the laccases and the substrates. ND, not determined.

	2,6-DMP		Syringic acid		Methyl syringate	
	pH 4.5 E° = 0.53 V	pH 6 E° = 0.40 V	pH 4.5 E° = 0.57 V	pH 6 E° = 0.51 V	pH 4.5 E° = 0.69 V	pH 6 E° = 0.65 V
rMaL (E° = 0.48 V)						
ΔE° (V)	− 0.05	0.08	− 0.09	− 0.03	− 0.21	− 0.17
K_m (μM)	18 ± 1	9.5 ± 0.9	122 ± 11	132 ± 22	ND	ND
V_{max} (dA min^{-1}·$nmol^{-1}$)	126 ± 2	119 ± 1	3.5 ± 0.1	12.1 ± 0.6	ND	ND
TaLcc1 (E° = 0.51 V)						
ΔE° (V)	− 0.02	0.11	− 0.06	0	− 0.18	− 0.14
K_m (μM)	45 ± 4	5.8 ± 0.6	128 ± 4	61 ± 4	ND	ND
V_{max} (dA min^{-1}·$nmol^{-1}$)	99 ± 2	87 ± 1	3.5 ± 0.1	2.7 ± 0.1	ND	ND
ThL (E° = 0.78 V)						
ΔE° (V)	0.25	0.38	0.21	0.27	0.09	0.13
K_m (μM)	18 ± 1	6.3 ± 1.3	35 ± 6	17 ± 4	168 ± 19	50 ± 16
V_{max} (dA min^{-1}·$nmol^{-1}$)	193 ± 3	91 ± 2	8.3 ± 0.4	2.0 ± 0.1	21 ± 1	2.6 ± 0.2
	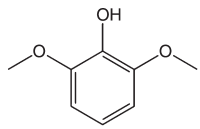		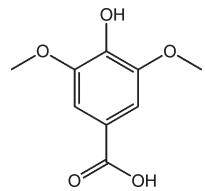		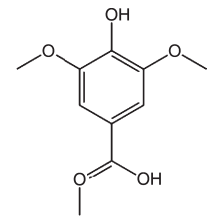	

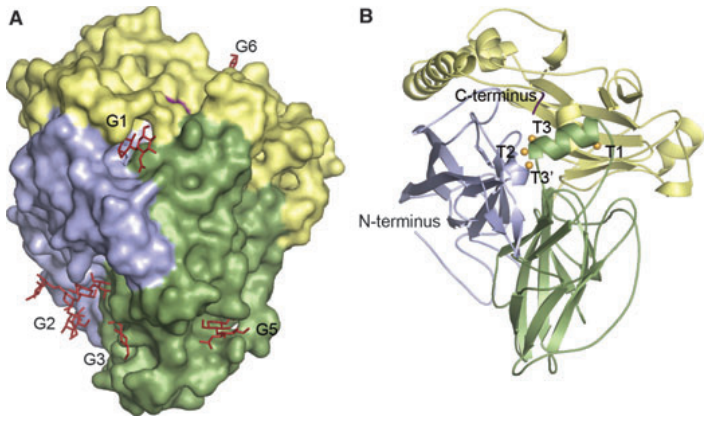

Fig. 1. (A) The crystal structure of TaLcc1 as a surface model. Domain A is presented in blue, domain B in green, and domain C in yellow. The N-glycans are shown as red sticks. Glycans are named as G1 on Asn89, G2 on Asn202, G3 on Asn217, G4 on Asn247 (on the other side of the molecule), G5 on Asn290, and G6 on Asn376. (B) Cartoon representation of TaLcc1. The catalytic coppers are shown in orange, and the C-terminal plug in purple.

scopic features. The T1 copper is responsible for the characteristic blue colour of these enzymes, and has strong absorption at 600 nm. The T1 and T2 coppers are paramagnetic, and can be detected by EPR spectroscopy. The T3 coppers form an antiferromagnetically coupled dinuclear copper–copper pair, and are therefore EPR silent, although these coppers cause absorbance at 330 nm. The loops surrounding the T1 copper form the phenolic substrate-binding site of the enzyme, whereas the T2 and the T3-pair coppers form the trinuclear site that is responsible for binding and reduction of the molecular oxygen. The reduction of oxygen to two water molecules requires the transfer of four electrons [26,27]. The rate-limiting step for the catalysis is apparently the transfer of the first electron from the substrate to the T1 copper in laccase. The suitability of a chemical compound as a laccase substrate depends on two factors. First, the substrate must dock at the T1 copper site, which is mainly determined by the nature and position of substituents on the phenolic ring of the substrate. Second, the redox potential ($E°$) of the substrate must be low enough, as the rate of the reaction has been shown to depend on the difference between the redox potentials of the enzyme and the substrate ($\Delta E°$) [28–31].

This study presents the crystal structure of a novel laccase (TaLcc1) from the ascomycete fungus *Thielavia arenaria* [32]. The molecular mass of the enzyme is $\sim$ 80 kDa (based on SDS/PAGE), and it shows multiple bands in IEF. The pH optimum is 5.5, but the enzyme retains substantial activity at pH 7. The three-dimensional structure of TaLcc1 shows both similarities to and differences from the analogous structures of the ascomycete laccase (asco-laccase) MaL, thus giving a comprehensive view of the structure and function of asco-laccases.

Results and Discussion

Overall structure

The crystal structure of TaLcc1 was solved to 2.5-Å resolution from pseudomerohedrally twinned crystals by molecular replacement, using the recombinant MaL expressed in *Trichoderma reesei* [rMaL; Protein Data Bank (PDB) code 2Q9O] [33] as a model. The real space group was $P2_1$, and it was mimicking orthorhombic (β = 90.3°). This led us to the solution with four molecules in an asymmetric unit, with a Matthews coefficient probability of 2.61 $A^3 \cdot Da^{-1}$ and a solvent content of 52.9%. Interestingly, molecules A and B (and C and D) formed a similar weak dimer as previously reported for rMaL [33]. Thus, the asymmetric unit contained two weak TaLcc1 dimers (Fig. 1).

The crystal structure of TaLcc1 contained 564 amino acids. The overall structure was similar to that of other fungal laccases, especially the only known asco-laccase structure from *M. albomyces* [25]. Protein monomers of the two asco-laccases could be superimposed with an rmsd of 0.65 Å for 558 Cα atoms. The fold is composed of three cupredoxin-like domains, called A (1–160), B (161–340), and C (340–564) (Fig. 1A,B), or sometimes referred to in the literature as domains I, II, and III. In TaLcc1, three disulfide bridges located in domain A (Cys5–Cys13), in domain B (Cys298–Cys332) and between domains A and C (Cys115–Cys545) stabilize the fold.

Most laccases are glycoproteins, with typically 3–10 glycosylation sites per monomer, although the functional role of the carbohydrates is not clear. Glycosylation has been suggested to be involved, for example, in the stabilization of the catalytic centre, giving protection against hydrolysis, and improving the

thermostability of the enzyme [34]. On the basis of the sequence of TaLcc1, there are eight putative N-glycosylation sites (Asn89, Asn202, Asn217, Asn247, Asn290, Asn337, Asn376, and Asn396), and carbohydrate residues were found on six of these sites (Asn89, Asn202, Asn217, Asn247, Asn290, and Asn376) in our crystal structure (Fig. 1A). The carbohydrate composition slightly varied between the molecules in the asymmetric unit; however, the glycans attached to Asn89 (G1 in Fig. 1A) and to Asn202 (G2 in Fig. 1A) were consistent in all four molecules. These two glycans seem to have a clear stabilizing effect on the multidomain protein structure. The glycan on Asn89 was located alongside the C-terminal tail between all three domains (Fig. 2A), and had two hydrogen bonds with Ser180 and Asn555. The glycan on Asn202 was in the groove between the β-barrels of domains A and B (Fig. 2B), and had six hydrogen bonds, three to the main chain carbonyls at Asn6, Leu168, and Val170, and three to the side chains of Arg11, Arg71, and Tyr216.

The catalytic centres were arranged in similar way as previously reported for MaL [25]. In the mononuclear centre, the T1 copper was coordinated to two ND1 atoms of His residues. The residues in the axial positions of the mononuclear centre were Leu and Ile. The trinuclear centre had two type 3 coppers (T3 and T3′), each being coordinated to three nitrogen atoms of His residues. The T2 copper was coordinated to two nitrogens of His residues. On the basis of the electron density, we refined one oxygen atom (probably a hydroxide) between the type 3 coppers in molecules B, C and D in the asymmetric unit of the crystal structure. However, the electron density among the coppers in molecule A was stronger than in the other molecules, and had a slightly elliptic shape towards the T2 copper. On the basis of these observations, we decided to refine a dioxygen molecule at this site. Another oxygen atom (most likely a hydroxide or a water molecule) was coordinated to the T2 copper on the opposite side (in the T2 solvent channel). No chloride was observed, even though the purified enzyme was in Tris/HCl buffer. In the crystal structure of MaL/rMaL, a chloride is bound to the T2 copper, whereas in other published laccase crystal structures, an oxygen atom, most likely in a hydroxide ion, is reported to be here.

T2 solvent channel

The water channel leading to the trinuclear centre from the side of the T2 copper, between domains A and C, can be found in all fungal laccases except in in rMaL, where His98 blocks the access. The T2 cavity is surrounded by acidic Asp residues (Fig. 3), which have been suggested to provide the protons required for dioxygen reduction in Fet3p multicopper oxidase [35]. In our TaLcc1 structure, His98 was replaced by Arg99, orientated such that it formed the surface of the solvent channel. Therefore, the access through the channel was unhindered in TaLcc1 (Fig. 3A). It is possible that His98 in rMaL may also rotate to another conformation to open the T2 channel (Fig. 3B). On the basis of protein structure libraries, the 'open conformation' would be the second most favoured conformation. On the other hand, we did not observe any trace of the movements on the His98 residue in our MaL/rMaL

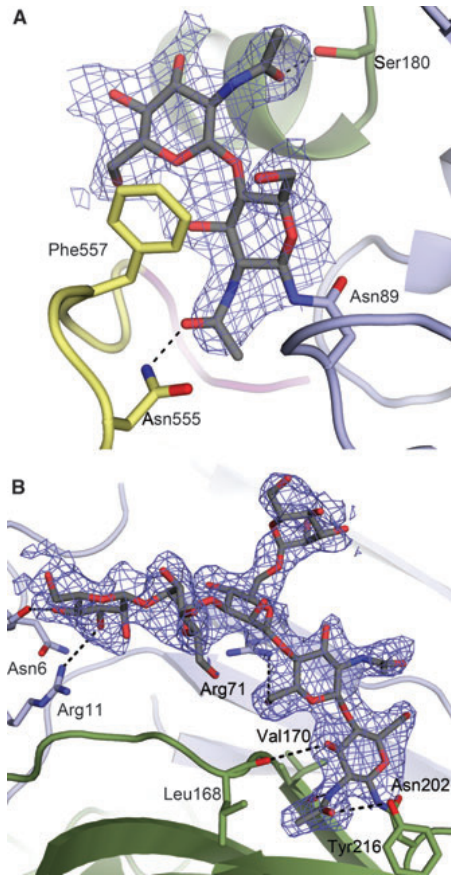

Fig. 2. Stabilizing carbohydrates of TaLcc1. Domain A is presented in blue, domain B in green, and domain C in yellow. (A) The glycan on Asp89 stabilizes the C-terminal tail (marked in purple). (B) The glycan on Asp202 is located on the groove between domain A and domain B. The $2F_o - F_c$ electron density for the carbohydrates is presented in cyan, contoured at 1σ.

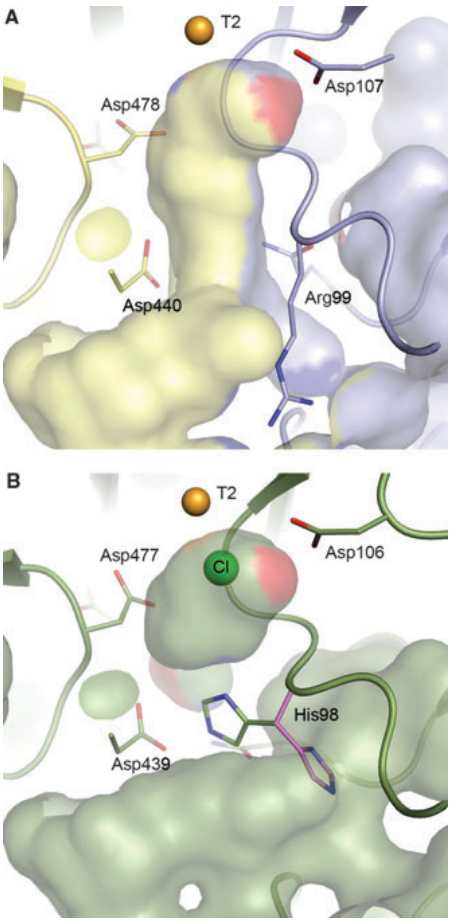

Fig. 3. T2 solvent channels leading into the trinuclear centre of asco-laccases. (A) The open solvent channel in TaLcc1. The cavity is formed between domain A (blue) and domain C (yellow). (B) The closed solvent channel in rMaL. His98 (corresponding to Arg99 in TaLcc1) blocks the solvent channel in rMaL. The putative open conformation of His98 is shown in purple. In the rMaL structure, the chloride is located in the upper cavity.

crystal structures. In our near-atomic crystal structure of rMaL, His98 exists in its oxidized form, possibly because of the oxidative stress [33]. The oxidation of the His residues probably affects its ability to change the side chain conformation, which may have implications for the catalytic function of this laccase.

Role of the C-terminus

In addition to the T2 solvent channel, a so-called T3 solvent channel is generally reported in basidiomycete laccases. The T3 solvent channel gives the solvent access to the trinuclear centre. However, the channel is blocked by the C-terminal end of the amino acid chain in MaL/rMaL [25,33]. Similarly, in the structure of TaLcc1, the last four amino acids (DSGL) penetrate inside the channel. This is known as a C-terminal plug or a C-terminal tail. On the basis of the crystal structure, the mature TaLcc1 enzyme lacks 40 residues at the N-terminus and 13 residues at the C-terminus as compared with the coded sequence. It has been previously reported that the gene sequence of rMaL codes for 623 residues, but the secreted mature enzyme lacks 50 residues at the N-terminus and 14 residues at the C-terminus [36]. The C-terminal extension containing the last 14 (13 in TaLcc1) residues is post-translationally cleaved, and thus the active forms of both enzymes have DSGL as the last four amino acids penetrating into the channel.

The C-terminal processing has been reported for asco-laccases of different origins [37–39]; furthermore, the C-terminus of the mature asco-laccases is highly conserved, suggesting that the DSGL/V/I plug is most likely a characteristic feature of asco-laccases. Basidiomycete laccases do not generally have this type of C-terminus. However, *R. lignosus* laccase (RlL) [13] has a C-terminal DSGLA sequence. Among the known basidiomycete laccases, RlL is phylogenetically the closest to asco-laccases. Although the last amino acids of RlL are not visible in the crystal structure, it is unlikely that the C-terminus of RlL would be long enough to form such a plug, as the last visible amino acid (Asn494) is located on the surface of the molecule and is rather far away from the trinuclear site. Therefore, the C-terminal sequence of RlL might be more of an evolutionary relic than a functional feature of the enzyme.

The actual role of the C-terminus in asco-laccases has been unclear. However, we have recently shown that a mutation in the C-terminus of rMaL affects both the activity and the stability of the enzyme [40]. The Leu559 → Ala mutation greatly reduced the turnover number for ABTS, whereas the turnover number for the phenolic substrates was not significantly altered. In addition, deletion of the four last amino acids (delDSGL) of rMaL resulted in a practically inactive form of the enzyme [40]. Therefore, it is obvious that the C-terminal amino acids are critical for the function of asco-laccases. Furthermore, the C-terminal extension (the amino acids after the cleavage site) has been shown to affect the secretion process and folding of asco-laccases [41].

Very recently, studies on a CotA laccase from *B. subtilis* (BsL) have provided evidence for Glu498 near the T3 coppers participating in the catalytic

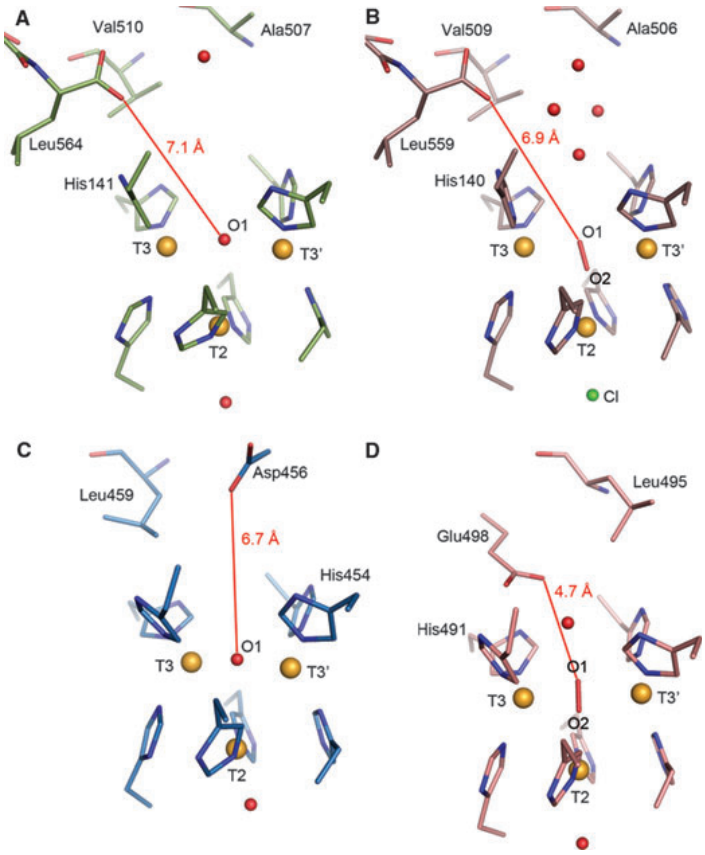

Fig. 4. The trinuclear centres of (A) TaLcc1, (B) rMaL, (C) TvL, and (D) BsL. The distance of the putative catalytic carboxyl group from the oxygen species between the T3 coppers is shown.

function of the enzyme, possibly by promoting proton transfer [42,43]. The fungal laccase structures have no Glu or Asp in this position, but basidiomycete fungal laccases have a conserved Asp in close proximity, i.e. Asp456 in *T. versicolor* laccase. In asco-laccases, the only acidic residue in the T3 solvent cavity that is close enough to assist in the proton transfer is the carboxylate from the C-terminus. The C-terminal carboxylate group of asco-laccases and the conserved Asp of the basidiomycete laccases are both ~ 7 Å from the oxygen species located between the T3 coppers. Glu498 of BsL is 4.7 Å from this oxygen (Fig. 4). It is plausible that asco-laccases use the C-terminal carboxylate group and basidiomycete laccases use the conserved Asp to assist proton transfer for reducing the molecular oxygen. Nevertheless, the continuous flow of protons from the phenolic substrate might come through the so-called SDS gate, which is conserved in asco-laccases but not detected in basidiomycete laccases or the *B. subtilis* CotA laccase. The SDS gate is formed by two Ser residues and one Asp residue, and it is thought to be involved in proton transfer from the T1 site to the trinuclear centre [33]. In TaLcc1, Ser143, Ser511 and Asp561 form the SDS gate, which possibly assists the proton flow. Laccases from different organisms might thus have adopted different strategies to facilitate proton transfer for the dioxygen reduction.

Oxidation of phenolic substrates

The substrate-binding pocket of TaLcc1 is similar to that in MaL, but there are clear differences in both the size and the shape of the pocket (Fig. 5A,B). Leu297 in TaLcc1 (Ala297 in MaL) narrows the cavity as compared with MaL, whereas Pro195 and Val428 (Phe194 and Phe427 in MaL) make the cavity in TaLcc1 wider in the other direction. In addition, the loop with Val428 has an additional Ile427 in TaLcc1. This

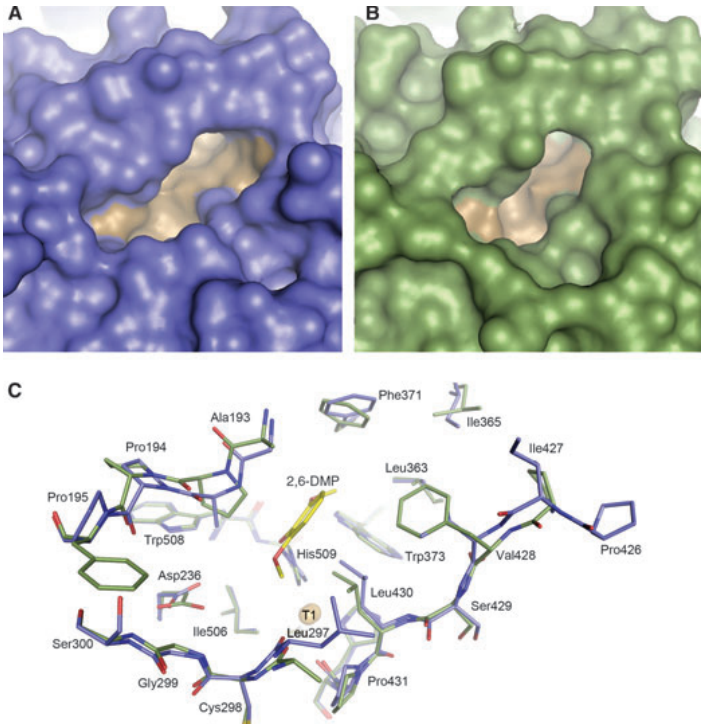

Fig. 5. (A, B) The substrate-binding pockets of (A) TaLcc1 and (B) rMaL. (C) Superimposed amino acids forming the substrate-binding pockets. TaLcc1 is shown in blue, rMaL in green, and 2,6-DMP from the complex structure (PDB code 3FU8) in yellow. The amino acids of TaLcc1 are labelled.

loop resembles 'the extended jut' reported in LacB of *Trametes* sp., which was also suggested to be involved in substrate recognition [44].

In TaLcc1, 10 hydrophobic residues (Ala193, Leu297, Leu363, Phe371, Trp373, Ile427, Val428, Leu430, Trp508, and His509) and one hydrophilic residue, Asp236, form the binding pocket. The most evident difference between MaL and TaLcc1 is in this putative catalytic amino acid: TaLcc1 has an Asp236, instead of the Glu235 observed in MaL. Most basidiomycete laccases, such as *T. versicolor*, *L. tigrinus* and *C. cinereus* laccases, have Asp residues here. In the crystal structure of the basiodiomycete *T. hirsuta* laccase (PDB code 3FPX), the corresponding residue is an Asn, and it has been suggested that this contributes to the high catalytic constants of *T. hirsuta* [18]. However, the purified laccase from *T. hirsuta* (ThL) (UniProt Knowledgebase accession number Q02497) used in our experiments has an Asp here [45].

In order to understand the oxidation of phenolic compounds in the binding pockets of laccases, the kinetic behaviour of TaLcc1, rMaL and ThL on three phenolic compounds [2,6-dimethoxyphenol (2,6-DMP), syringic acid, and methyl syringate] was studied (Table 1). The dimethoxy phenolic substrates have different *para*-substituents and different redox potentials. On the basis of our crystal structure of rMaL with 2,6-DMP [46], and the *T. versicolor* laccase (TvL) complex structure with 2,5-xylidine [11], the *para*-substituents would point out from the binding pocket and therefore not affect the substrate binding. The rate of laccase-catalysed reactions is thought to increase as the redox potential difference (ΔE°) between the T1 copper and the substrate increases. In TaLcc1, the redox potential of the T1 copper is slightly higher (0.51 V) than that in rMaL (0.48 V), but not as high as in ThL (0.78 V); thus, it would be expected that the kinetic data for TaLcc1 would fit in between the data of rMaL and ThL. However, our kinetic data clearly show that this is not the case, suggesting that the redox potential difference is not the only factor contributing to the rate of substrate oxidation (Table 1).

The kinetics of substrate oxidation by laccases has also been shown to be pH-dependent [47]. At higher pH values, phenolic substrates have lower E° values, whereas E° for the T1 copper of laccases seems to be unaffected by varying pH [28]. As consequence, when ΔE° increases at the higher pH, the reaction rate is increased, but the inhibitory effect of hydroxide also increases. A typical feature of basidiomycete laccases is

their acidic pH optima, whereas asco-laccases generally work in a more neutral range with phenolic compounds [48,49]. Therefore, kinetic studies were carried out at pH 4.5, which is more optimal for ThL, and at pH 6.0, which is, in general, more optimal for TaLcc1 and rMaL (Fig. S1). Because both the pH dependence and the difference in redox potential affect the kinetics of the laccases, we concluded that rMaL and TaLcc1 were able to oxidize syringic acid at pH 6.0, mainly owing to the favourable pH, whereas ThL could oxidize the same substrate, mainly because of the large difference in redox potential. However, the effect of the difference in redox potential outweighs the effect of pH for substrates with high $E°$, such as methyl syringate. Oxidation of methyl syringate was only possible with the high redox potential ThL, whereas the kinetic parameters for this substrate could not be determined with TaLcc1 or rMaL at either pH value (Table 1).

Interestingly, TaLcc1 showed a lower K_m for 2,6-DMP at pH 6.0 than at pH 4.5 (Table 1). Despite the small difference in redox potentials of the two asco-laccases and their very similar pH optimum profiles, the affinity of TaLcc1 for 2,6-DMP was lower than the affinity of rMaL for the same substrate at pH 4.5. The similar pH profiles and $\Delta E°$ values for the two asco-laccases do not explain the three-fold increase in reaction rate of rMaL with syringic acid at pH 6 as compared with pH 4.5. These differences in kinetic behaviour between TaLcc1 and rMaL must therefore be attributable to the variations in several residues forming the binding pocket, most likely Asp236, Ala193 and Val428 observed in TaLcc1 instead of Glu235, Pro192 and Phe427 observed in rMaL. Our mutagenesis studies with MaL have demonstrated that Glu235 → Asp mutation of the catalytic residue clearly increases the K_m value for phenolic substrates while not affecting the k_{cat} value. Furthermore, both the K_m and k_{cat} values were clearly affected by the Glu235 → Thr mutation, suggesting the importance of the carboxylic group for the catalytic activity [46]. In addition, Phe427 in rMaL (Val428 in TaLcc1) might be involved in placing substrate molecules into the correct orientation for oxidation. In *T. hirsuta*, the loops forming the substrate-binding pocket are completely different, possibly accounting for the clear differences in reaction kinetics between basidiomycete laccases and asco-laccases.

Dimerization

In the TaLcc1 crystal structure, molecules A and B (and C and D) of the asymmetric unit form a weak dimer (Fig. 6). On the basis of calculations performed

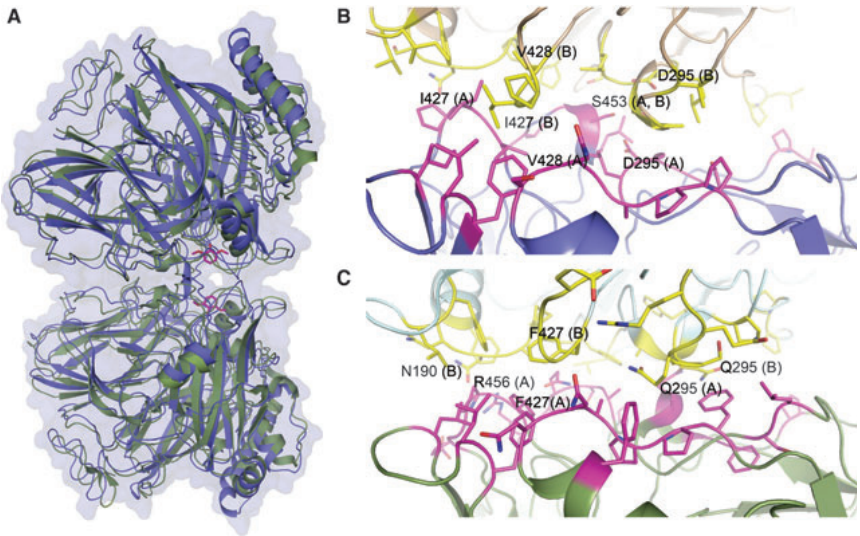

Fig. 6. (A) Cartoon representation of dimers of TaLcc1 (blue) and rMaL (green). 2,6-DMP ligands (purple) are presented as they are in the rMaL complex structure (PDB code 3FU8). A surface representation of TaLcc1 (light blue) shows a small central channel that provides access for the substrates. (B, C) The contact amino acids at the dimeric interface in TaLcc1 (B) and rMaL (C). The residues from molecule A are shown in purple, and those from molecule B in yellow. The hydrogen bonding residues (according to Protein Interfaces, Surfaces and Assemblies) have been labelled, as have the hydrophobic residues with the closest contacts.

with the Protein Interfaces, Surfaces and Assemblies service [50–52], the buried surface area for the weak dimers, AB and CD, is 3.2% (658 Å^2) and 3.3% (667 Å^2) of the total surface area, respectively. In this weak dimer, the loop areas surrounding the phenolic substrate-binding pockets are packed together (Fig. 6A). Similar dimerization has been reported in the crystal structure of MaL [33]. In MaL, one of the key residues for the dimeric interaction is Phe427, located at the edge of the substrate-binding pocket. This residue might be involved in the orientation or the docking of the substrate molecules. In MaL, the Phe residues from two molecules are packed face-to-face. In TaLcc1, the corresponding loop is longer, and the interacting residues are Ile427 and Val428 (Fig. 6B). As a consequence, the T1–T1 copper distance is slightly longer in TaLcc1 (28 Å) than in MaL (27 Å), and the surface contact area is also slightly smaller (667 Å^2) than that on MaL (796 Å^2 for 2Q9O).

It is possible that the weak dimers of MaL and TaLcc1 are the so-called 'transient dimers', which exist in solution as a mixture of monomers and dimers in a concentration-dependent manner [53]. It is noteworthy that the dimeric composition in MaL and TaLcc1 is very similar, suggesting that the ability to form dimers may have functional meaning. Interestingly, the two substrate-binding sites are packed against each other, and there is a shared cavity in the interface of the dimer. This cavity is enclosed in the MaL structure, whereas in the TaLcc1 structure there is a clear solvent channel in the interface between protein molecules that provides free access of the substrate molecules to the binding sites (Fig. 6A). However, the cavity itself is more compact in TaLcc1 than in MaL, owing to the loop containing Ile427 and Val428. The other narrow solvent channel reported earlier for rMaL is also visible in TaLcc1 [46]. The observed dimer in the crystalline state favours smaller phenolic substrates without large substituents in the *para*-position. The docking simulations based on the crystal structure for TaLcc1 reveal that substrates with large groups at the *para*-position clash with the loop containing Ile427 and Leu428. The corresponding loop is shorter in MaL, and the cavity is also more spacious.

Industrial utilization

Laccases have wide reaction capabilities and possess great biotechnological potential, because of their broad substrate specificity. Laccases can be utilized in many industrial applications, including biopulping, textile dye bleaching, bioremediation, biological fuel cells, and sensors. The stability and activity over broad pH and temperature ranges are desired properties for industrial enzymes. With respect to industrial applications, the ascomycete fungal laccase TaLcc1 is an efficient enzyme, particularly in denim bleaching, even at high temperatures and at neutral pH [32].

In general, asco-laccases possess a wider optimal pH range than basidiomycete laccases; however, the catalytic ability of asco-laccases in less acidic conditions has not yet been fully clarified on the basis of the available laccase structures. It could be that the adaptation of slightly different methods for proton transfer in asco-laccases and basidiomycete laccases (and in bacterial laccases) is responsible for the differences in the pH optimum range of laccases. In addition, the trinuclear site in asco-laccases is more protected, owing to the C-terminal plug; this might reduce the effect of hydroxide inhibition. Both TaLcc1 and MaL are also rather thermostable as compared with many other laccases. The stabilization of both the N-termini and C-termini of TaLcc1 and MaL might be a reason for the higher thermal stability. The extended C-terminus of asco-laccases is buried inside the solvent channel, and the extended N-terminus is stabilized by an additional disulfide bridge. In addition, both termini interact with carbohydrates bound to the protein structure.

Asco-laccases typically have middle redox potentials (TaLcc1, 0.51 V), whereas many basidiomycete laccases have very high redox potentials (ThL, 0.78 V), resulting in enhanced oxidation power. In the future, rational design methods could be used for tuning the redox potential of asco-laccases, or to increase the stability and the optimal pH range of high redox potential basidiomycete laccases. However, more studies are needed to understand how the enzyme structure contributes to the industrially desired properties.

Experimental procedures

Purification

TaLcc1 was produced at Roal Oy (Rajamäki, Finland), with *Tr. reesei* as host [32]. The culture supernatant was concentrated, buffer-exchanged, applied to a weak anion exchange column (DEAE Sepharose FF) in 5 mM Tris/HCl buffer (pH 8.5), and eluted with a linear 0–100 mM sodium sulfate gradient. Active fractions were pooled on the basis of ABTS activity, and were concentrated and desalted (Vivaspin, MWCO 10 000 Da). Typically, the laccase was further purified with a high-resolution anion exchange column (Resource Q) pre-equilibrated in 5 mM Tris/HCl

buffer (pH 8.5). The bound proteins were eluted with a linear sodium sulfate gradient (0–100 mM). Active fractions were eluted at sodium sulfate concentrations between 5 and 40 mM, and concentrated. Subsequently, the buffer was changed to Tris/HCl (20 mM, pH 7.2). The protein yield from the purification was 6%, and the purification factor was 1.5.

MaL was overproduced in *Tr. reesei*, and purified basically as described previously [54]. ThL, assigned with UniProt Knowledgebase accession number Q02497 [45], was produced in its native host and purified in two chromatographic steps, as described previously [55].

Crystallization

TaLcc1 was crystallized at room temperature with the hanging drop vapour diffusion method. Two microlitres of protein solution at a concentration of 9 mg·mL^{-1} and 2 μL of crystallization solution were equilibrated against 500 μL of reservoir solution. Initial screens were made with Crystal Screen I by Hampton Research. Optimization of the molecular weight of poly(ethylene glycol) and its concentration, together with pH, led us to the final crystallization condition of 7.5% poly(ethylene glycol) 3350, 0.2 M ammonium sulfate, and 0.1 M sodium acetate (pH 4.4). The streak seeding method with an equilibration time of ~ 10 h was used to obtain better-quality crystals. The crystals grew as thin plates, which made them difficult to handle. The crystals were approximately 0.3–1 mm long and 0.15–0.5 mm wide, and the thickness of the crystals was always under 0.1 mm.

Data collection and structure refinement

Before data collection, TaLcc1 crystals were quickly soaked in a cryoprotectant solution containing the reservoir solution with 25% glycerol. The crystal was then picked up with nylon loops and flash-frozen in liquid nitrogen. Data were collected at 100 K with synchrotron radiation at the European Synchrotron Radiation Facility (Grenoble) on beamline ID14-1, using an ADSC Q210 charge-coupled device detector. The data were indexed and integrated in MOSFLM [56], and scaled to 2.5-Å resolution in SCALA [57] from CCP4 [58]. The structure factors were created with TRUNCATE [59] from CCP4. A summary of the processing statistics is given in Table 2. The rather high R_{merge} might be attributable to twinning or, additionally, to anisotropic diffraction patterns of the crystal.

The data were analysed with XTRIAGE from the PHENIX package [60]. The suggested lattice was monoclinic, but the highest possible lattice seemed to be orthorhombic. The multivariate *L*-tests strongly indicated that the data were twinned. The *Z*-score was 10.9, whereas the value should be under 3.5 for good-quality to reasonable-quality data. The twin operator for this case was (h, $-k$, $-l$), and the estimated twin fraction was about 0.3 (Table 2). In addition, we also noticed a rather large off-origin peak, indicating some pseudotranslational symmetry that is most likely involved in the twinning with noncrystallographic symmetry.

Table 2. Summary of processing and refinement statistics. Values in parentheses are for highest-resolution shells. $R_{merge} = \sum_h \sum_I |I_{hI} - \langle I_h \rangle| / \sum_h \sum_I \langle I_h \rangle$. $R_{pim} = \sum_h (1/n_h - 1)^{1/2} \sum_I |I_{hI} - \langle I_h \rangle| / \sum_h \sum_I \langle I_h \rangle$.

Data collection	
Wavelength (Å)	0.934
No. of images	360
Crystal–detector distance (mm)	239.3
Oscillation range (°)	0.5
Space group	$P2_1$
Unit cell	a = 61.3, b = 178.9, 118.1, b = 90.3
Resolution range (Å)	42.6–2.5 (2.6–2.5)
No. of reflections	334 560 (49 270)
No. of unique reflections	87 766 (12 787)
Completeness (%)	99.9 (99.9)
I/σ (I)	5.8 (2.9)
Multiplicity	3.8 (3.9)
R_{merge}	25.8 (44.1)
R_{pim}	15.3 (26.0)
Analysis	
Statistics independent of twin laws	
<I^2 > /<I>^2	1.99
<F>^2/<F^2>	0.83
<|E^2-1|>	0.67
<|L|>, <L^2>	0.38, 0.20
Z-score *L*-test	10.9
Twin fraction estimated	0.30
Twin law	$h, -k, -l$
Refined twin fraction	0.36
Refinement	
R_{work}	18.1
R_{free}	22.4
rmsd bond length from ideal (Å)	0.009
rmsd bond angles from ideal (°)	1.053
Ramachandran plot	
Favoured (%)	92.9
Allowed (%)	7.0
Outlier (%)	0.1

The structure was solved by molecular replacement with the rMaL structure (75% sequence identity) as a model. Molecular replacement was performed with PHASER [61] from the CCP4 package and the rMaL (PDB code 2Q9O) coordinates as a model. Only in space group $P2_1$ were rotation and translation solutions found that showed reasonable crystal packing. The *R*-values for the first round of refinement were R = 26.7% and R_{free} = 34.9%. When a twin operator was included, *R*-value and R_{free}-value were decreased to 19.2% and 25.2%, respectively. Refinement of the model and twin fraction were carried out with PHENIX, and model building in COOT [62]. The final *R*-values after the refinement were R = 18.1% and R_{free} = 22.4%, and the twin fraction was refined to 0.36. Despite the twinning,

a surprisingly good-quality and continuous electron density map was observed. Noncrystallographic symmetry restraints were used during the refinement, and we also tried to release them, but this resulted in high *B*-factors for atoms in molecules C and D. Validation was performed with SFCHECK [63] from the CCP4 package, with 92.9% of all residues being in the most favourable region of the Ramachandran plot (Table 2).

Kinetic data

Kinetic constants (K_m and V_{max}) for rMaL, TaLcc1 and ThL were determined on 2,6-DMP, syringic acid, and methyl syringate, at both pH 4.5 and pH 6.0, in 25 mM succinate buffer and 40 mM Mes buffer, respectively (Table 1). Kinetic measurements were performed in microtitre plates with a Varioskan kinetic plate reader (Thermo Electron Corporation, Waltham, MA, USA). The reactions were started by addition of substrate, and the rate of substrate oxidation was measured by monitoring the change in absorbance over 5 min. All of the measurements were performed in duplicate, with eight substrate concentrations (0.008–1.333 mM for 2,6-DMP and syringic acid; 0.008–2.800 mM for methyl syringate). The kinetic parameters were obtained by curve-fitting analysis with GRAPHPAD PRISM 4.01 (GraphPad Software). The pH optima of the three laccases were measured, with a substrate concentration of 1.7 mM, for 2,6-DMP, syringic acid and methyl syringate in McIlvaine's buffer system at pH levels ranging from 2 to 8.

Acknowledgements

We are grateful to M. Paloheimo from Roal Oy for providing us with samples of TaLcc1. The ESRF is thanked for provision of synchrotron facilities. We also thank the staff members at beamline ID14-1 for their skilled assistance, and B. Hillebrant-Chellaoui at VTT for skilful help with the TaLcc1 purification. Roal Oy and the Academy of Finland (Project 115085) supported the work at Joensuu, and part of the VTT work was carried out with financial support from the Marie Curie EU-project 'Enzymatic tailoring of protein interactions and functionalities in food matrix', PRO-ENZ (MEST-CT-2005-020924), and from the National Technology Agency of Finland, Tekes project 40522/02.

References

1 Messerschmidt A, Ladenstein R & Huber R (1992) Refined crystal structure of ascorbate oxidase at 1.9 Å resolution. *J Mol Biol* **224**, 179–205.
2 Lindley PF, Card G, Zaitseva I, Zaitsev V, Reinhammar B, Selin-Lindgren B & Yoshida K (1997) An X-ray structural study of human ceruloplasmin in relation to ferroxidase activity. *J Biol Inorg Chem* **2**, 454–463.
3 Roberts SA, Wildner GF, Grass G, Weichsel A, Ambrus A, Rensing C & Montfort WR (2003) A labile regulatory copper ion lies near the T1 copper site in the multicopper oxidase CueO. *J Biol Chem* **278**, 31958–31963.
4 Taylor A, Stoj CS, Ziegler L, Kosman DJ & Hart J (2005) The copper–iron connection in biology: structure of a metallo-oxidase Fet3p. *Proc Natl Acad Sci USA* **102**, 15459–15464.
5 Smith AW, Camara-Artigas A, Wang M, Allen JP & Francisco WA (2006) Structure of phenoxazinone synthase from Streptomyces antibioticus reveals a new type 2 copper center. *Biochemistry* **45**, 4378–4387.
6 Thuesen MH, Farver O, Reinhammar B & Ulstrup J (1998) Cyclic voltammetry and electrocatalysis of the blue copper oxidase *Polyporus versicolor* laccase. *Acta Chem Scand* **52**, 555–562.
7 Blanford CF, Heath RS & Armstrong FA (2007) A stable electrode for high-potential, electrocatalytic O_2 reduction based on rational attachment of a blue copper oxidase to a graphite surface. *Chem Commun* **17**, 1710–1712.
8 Xu F (2005) Applications of oxidoreductases: recent progress. *Ind Biotechnol* **1**, 38–50.
9 Rodríguez Couto S & Toca Herrera JL (2006) Industrial and biotechnological applications of laccases: a review. *Biotechnol Adv* **24**, 500–513.
10 Ducros V, Brzozowski AM, Wilson KS, Brown SH, Ostergaard P, Schneider P, Yaver DS, Pedersen AH & Davies GJ (1998) Crystal structure of the type-2 Cu depleted laccase from *Coprinus cinereus* at 2.2 A resolution. *Nat Struct Biol* **5**, 310–316.
11 Bertrand T, Jolivalt C, Briozzo P, Caminade E, Joly N, Madzak C & Mougin C (2002) Crystal structure of a four-copper laccase complexed with an arylamine: insights into substrate recognition and correlation with kinetics. *Biochemistry* **41**, 7325–7333.
12 Piontek K, Antorini M & Choinowski T (2002) Crystal structure of a laccase from the fungus *Trameters versicolor* at 1.90 Å resolution containing a full complement of coppers. *J Biol Chem* **277**, 37663–37669.
13 Garavaglia S, Cambria MT, Miglio M, Ragusa S, Iacobazzi V, Palmieri F, D'Ambrosio C, Scaloni A & Rizzi M (2004) The structure of *Rigidoporus lignosus* laccase containing a full complement of copper ions, reveals an asymmetrical arrangement for the T3 copper pair. *J Mol Biol* **342**, 1519–1531.
14 Lyashenko AV, Bento I, Zaitsev VN, Zhukhlistova NE, Zhukova YN, Gabdoulkhakov AG, Morgunova EY, Voelter W, Kachalova GS, Stepanova EV *et al.* (2006) X-ray structural studies of the fungal laccase from *Cerrena maxima*. *J Biol Inorg Chem* **11**, 963–973.

15 Lyashenko AV, Zhukova Y, Zhukhlistova N, Zaitsev V, Stepanova E, Kachalova G, Koroleva O, Voelter W, Betzel C, Tishkov V *et al*. (2006) Three-dimensional structure of laccase from *Coriolus zonatus* at 2.6 Å resolution. *Crystallogr Rep* **51**, 817–823.
16 Ferraroni M, Myasoedova NM, Schmatchenko V, Leontievsky AA, Golovleva LA, Scozzafava A & Briganti F (2007) Crystal structure of a blue laccase from *Lentinus tigrinus*: evidences for intermediates in the molecular oxygen reductive splitting by multicopper oxidases. *BMC Struct Biol* **7**, 60, doi:10.1186/1472-6807-7-6.
17 Matera I, Gullotto A, Tilli S, Ferraroni M, Scozzafava A & Briganti F (2008) Crystal structure of the blue multicopper oxidase from the whiterot fungus *Trametes trogii* complexed with p-toluate. *Inorg Chim Acta* **361**, 4129–4137.
18 Polyakov KM, Fedorova TV, Stepanova EV, Cherkashin EA, Kurzeev SA, Strokopytov BV, Lamzin VS & Koroleva OV (2009) Structure of native laccase from *Trametes hirsuta* at 1.8 A resolution. *Acta Crystallogr* **D65**, 611–617.
19 Reference withdrawn
20 Enguita FJ, Marçal D, Martins LO, Grenha R, Henriques AO, Lindley PF & Carrondo MA (2004) Substrate and dioxygen binding to the endospore coat laccase from *Bacillus subtilis*. *J Biol Chem* **279**, 23472–23476.
21 Li X, Wei Z, Zhang M, Peng X, Yu G, Teng M & Gong W (2007) Crystal structures of *E. coli* laccase CueO at different copper concentrations. *Biochem Biophys Res Commun* **354**, 21–26.
22 Komori H, Miyazaki K & Higuchi Y (2009) X-ray structure of a two-domain type laccase: a missing link in the evolution of multi-copper proteins. *FEBS Lett* **583**, 1189–1195.
23 Lawton TJ, Sayavedra-Soto LA, Arp DJ & Rosenzweig AC (2009) Crystal structure of a two-domain multicopper oxidase: implications for the evolution of multicopper blue proteins. *J Biol Chem* **284**, 10174–10180.
24 Skálová T, Dohnálek J, Østergaard LH, Østergaard PR, Kolenko P, Dusková J, Stepánková A & Hasek J (2009) The structure of the small laccase from *Streptomyces coelicolor* reveals a link between laccases and nitrite reductases. *J Mol Biol* **385**, 1165–1178.
25 Hakulinen N, Kiiskinen L-L, Kruus K, Saloheimo M, Paananen A, Koivula A & Rouvinen J (2002) Crystal structure of a laccase from *Melanocarpus albomyces* with an intact trinuclear site. *Nat Struct Biol* **9**, 601–605.
26 Solomon EI, Sundaram UM & Machonkin TE (1996) Multicopper oxidases and oxygenases. *Chem Rev* **96**, 2563–2606.
27 Solomon EI, Chen P, Metz M, Lee S-K & Palmer AE (2001) Oxygen binding, activation, and reduction to water by copper enzymes. *Angew Chem Int Ed* **40**, 4570–4590.
28 Xu F (1996) Oxidation of phenols, anilines, and benzenethiols by fungal laccases: correlation between activity and redox potentials as well as halide inhibition. *Biochemistry* **35**, 7608–7614.
29 Xu F, Shin W, Brown SH, Wahleithner JA, Sundaram UM & Solomon EI (1996) A study of a series of recombinant fungal laccases and bilirubin oxidase that exhibit significant differences in redox potential, substrate specificity, and stability. *Biochim Biophys Acta Protein Struct Mol Enzymol* **1292**, 303–311.
30 Xu F, Kulys JJ, Cuke K, Li K, Kristopaitis K, Deussen HW, Abbate E, Galinyte V & Schneider P (2000) Redox chemistry in laccase-catalyzed oxidation of N-hydroxy compounds. *Appl Environ Microbiol* **66**, 2052–2056.
31 Xu F, Deussen HW, Lopez B, Lam L & Li K (2001) Enzymatic and electrochemical oxidation of N-hydroxy compounds: redox potential, electron transfer kinetics, and radical stability. *Eur J Biochem* **268**, 4169–4176.
32 Paloheimo M, Valtakari L, Puranen T, Kruus K, Kallio J, Mäntylä A, Fagerström R, Ojapalo P & Vehmaanperä J (2006) Novel laccase enzyme and use thereof. European patent application WO/2006/032723.
33 Hakulinen N, Andberg M, Kallio J, Koivula A, Kruus K & Rouvinen J (2008) A near atomic resolution structure of a *Melanocarpus albomyces* laccase. *J Struct Biol* **162**, 29–39.
34 Rodger CJ, Blanford CF, Giddens SR, Skamnioti P, Armstrong FA & Gurr SJ (2010) Designer laccases: a vogue for high-potential fungal enzymes? *Trends Biotechnol* **28**, 63–72.
35 Quintanar L, Stoj C, Wang T-P, Kosman DJ & Solomon EI (2005) Role of aspartate 94 in the decay of the peroxide intermediate in the multicopper oxidase Fet3p. *Biochemistry* **44**, 6081–6091.
36 Kiiskinen L-L & Saloheimo M (2004) Molecular cloning and expression in *Saccharomyces cerevisiae* of a laccase gene from the ascomycete *Melanocarpus albomyces*. *Appl Environ Microbiol* **70**, 137–144.
37 Germann U, Muller G, Hunziker P & Lerch K (1988) Characterization of two allelic forms of *Neurospora crassa* laccase. Amino- and carboxyl-terminal processing of a precursor. *J Biol Chem* **263**, 885–896.
38 Fernandez-Larrea J & Stahl U (1996) Isolation and characterization of a laccase gene from *Podospora anserina*. *Mol Gen Genet* **252**, 539–551.
39 Bulter T, Alcalde M, Sieber V, Meinhold P, Schlachtbauer C & Arnold FH (2003) Functional expression of a fungal laccase in *Saccharomyces cerevisiae* by directed evolution. *Appl Environ Microbiol* **69**, 987–995.
40 Andberg M, Hakulinen N, Auer S, Saloheimo M, Koivula A, Rouvinen J & Kruus K (2009) Essential role of the C-terminus in *Melanocarpus albomyces* laccase for enzyme production, catalytic properties and structure. *FEBS J* **276**, 6285–6300.

41 Zumárraga M, Camarero S, Shleev S, Martínez-Arias A, Ballesteros A, Plou FJ & Alcalde M (2008) Altering the laccase functionality by in vivo assembly of mutant libraries with different mutational spectra. *Proteins* **71**, 250–260.
42 Chen Z, Durão P, Silva CS, Pereira MM, Todorovic S, Hildebrandt P, Bento I, Lindley PF & Martins LO (2010) The role of Glu^{498} in the dioxygen reactivity of CotA-laccase from *Bacillus subtilis*. *Dalton Trans* **39**, 2875–2882.
43 Bento I, Silva CS, Chen Z, Martins LO, Lindley PF & Soares CM (2010) Mechanisms underlying dioxygen reduction in laccases. Structural and modelling studies focusing on proton transfer. *BMC Struct Biol* **10**, 28, doi:10.1186/1472-6807-10-28.
44 Ge H, Gao Y, Hong Y, Zhang M, Xiao Y, Teng M & Niu L (2010) Structure of native laccase B from *Trametes* sp. AH28-2. *Acta Crystallogr* **F66**, 254–258.
45 Frasconi M, Favero G, Boer H, Koivula A & Mazzei F (2010) Bio-electrochemical characterisation of high and low redox potential laccases from fungal and plant origin. *Biochim Biophys Acta Proteins Proteom* **1804**, 899–908.
46 Kallio JP, Auer S, Jänis J, Andberg M, Kruus K, Rouvinen J, Koivula A & Hakulinen N (2009) Structure–function studies of a *Melanocarpus albomyces* laccase suggest a pathway for oxidation of phenolic compounds. *J Mol Biol* **392**, 895–909.
47 Xu F (1997) Effects of redox potential and hydroxide inhibition on the pH activity profile of fungal laccases. *J Biol Chem* **272**, 924–928.
48 Kiiskinen L-L, Viikari L & Kruus K (2002) Purification and characterization of a novel laccase from the ascomycete *Melanocarpus albomyces*. *Appl Microbiol Biotechnol* **59**, 198–204.
49 Chakroun H, Mechichi T, Martinez MJ, Dhouib A & Sayadi S (2010) Purification and characterizaion of a novel laccase from the ascomycete *Trichoderma atroviride*: application on bioremediation of phenolic compounds. *Process Biochem* **45**, 507–513.
50 Krissinel E & Henrick K (2005) Detection of protein assemblies in crystals. In *Lecture Notes in Computer Science* (Berthold MR ed), pp 163–174. Springer-Verlag, Berlin.
51 Krissinel E & Henrick K (2007) Inference of macromolecular assemblies from crystalline state. *J Mol Biol* **372**, 774–797.
52 Krissinel E (2009) Crystal contacts as nature's docking solutions. *J Comput Chem* **31**, 133–143.
53 Nooren MA & Thornton JM (2003) Structural characterization and functional significance of transient protein–protein interactions. *J Mol Biol* **325**, 991–1018.
54 Kiiskinen L-L, Kruus K, Bailey M, Ylosmaki E, Siika-aho M & Saloheimo M (2004) Expression of *Melanocarpus albomyces* laccase in *Trichoderma reesei* and characterization of the purified enzyme. *Microbiology* **150**, 3065–3074.
55 Rittstieg K, Suurnäkki A, Suortti T, Kruus K, Guebitz G & Buchert J (2002) Investigations on the laccase-catalyzed polymerization of lignin model compounds using size-exclusion HPLC. *Enzyme Microbial Technol* **31**, 403–410.
56 Leslie AGW (1992) Joint CCP4+ ESF-EAMCB. *Newslett Protein Crystallogr* **26**, 27–33.
57 Weiss M (2001) Global indicators of X-ray data quality. *J Appl Crystallogr* **34**, 130–135.
58 Collaborative Computational Project, Number 4 (1994) The CCP4 Suite: programs for protein crystallography. *Acta Crystallogr* **D50**, 760–763.
59 French GS & Wilson KS (1978) On the treatment of negative intensity observations. *Acta Crystallogr* **A34**, 517–525.
60 Adams PD, Grosse-Kunstleve RW, Hung L-W, Ioerger TR, McCoy AJ & Moriarty NW (2002) PHENIX: building new software for automated crystallographic structure determination. *Acta Crystallogr* **D58**, 1948–1954.
61 McCoy AJ, Grosse-Kunstleve RW, Adams PD, Winn MD, Storoni LC & Read RJ (2007) Phaser crystallographic software. *J Appl Crystallogr* **40**, 658–674.
62 Emsley P, Lohkamp B, Scott WG & Cowtan K (2010) Features and development of Coot. *Acta Crystallogr* **D66**, 486–501.
63 Vaguine AA, Richelle J & Wodak SJ (1999) SFCHECK: a unified set of procedures for evaluating the quality of macromolecular structure-factor data and their agreement with the atomic model. *Acta Crystallogr* **D55**, 191–205.

Supporting information

The following supplementary material is available:
Fig. S1. The pH activity profiles of rMaL, TaL and ThL for 1.7 mM 2,6-DMP, syringic acid and methyl syringate.

This supplementary material can be found in the online version of this article.

Please note: As a service to our authors and readers, this journal provides supporting information supplied by the authors. Such materials are peer-reviewed and may be re-organized for online delivery, but are not copy-edited or typeset. Technical support issues arising from supporting information (other than missing files) should be addressed to the authors.